Clim Dyn (2017) 49:143–161
DOI 10.1007/s00382-016-3332-z

400 Years of summer hydroclimate from stable isotopes in Iberian trees

Laia Andreu-Hayles[1,4] · Caroline C. Ummenhofer[2] · Mariano Barriendos[3,4] · Gerhard H. Schleser[5,6] · Gerhard Helle[5] · Markus Leuenberger[7] · Emilia Gutiérrez[8] · Edward R. Cook[1]

Received: 29 January 2016 / Accepted: 23 August 2016 / Published online: 4 November 2016

Abstract Tree rings are natural archives that annually record distinct types of past climate variability depending on the parameters measured. Here, we use ring-width and stable isotopes in cellulose of trees from the northwestern Iberian Peninsula (IP) to understand regional summer hydroclimate over the last 400 years and the associated atmospheric patterns. Correlations between tree rings and climate data demonstrate that isotope signatures in the targeted Iberian pine forests are very sensitive to water availability during the summer period, and are mainly controlled by stomatal conductance. Non-linear methods based on extreme events analysis allow for capturing distinct seasonal climatic variability recorded by tree-ring parameters and asymmetric signals of the associated atmospheric features. Moreover, years with extreme high (low) values in the tree-ring records were characterised by coherent large-scale atmospheric circulation patterns with reduced (enhanced) moisture transport onto the northwestern IP. These analyses of extremes revealed that high/low proxy values do not necessarily correspond to mirror images in the atmospheric anomaly patterns, suggesting different drivers of these patterns and the corresponding signature recorded in the proxies. Regional hydroclimate features across the broader IP and western Europe during extreme wet/dry summers detected by the northwestern IP trees compare favourably to independent multicentury sea level pressure and drought reconstructions for Europe. Historical records also validate our findings that attribute non-linear moisture signals recorded by extreme tree-ring values to distinct large-scale atmospheric patterns and allow for 400-year reconstructions of the frequency of occurrence of extreme conditions in late spring and summer hydroclimate.

Keywords Tree rings · Extreme analyses · Atmospheric circulation · Hydroclimate · Sea level pressure (SLP) · Old World Drought Atlas (OWDA) · Iberian Peninsula

✉ Laia Andreu-Hayles
lah@ldeo.columbia.edu

✉ Caroline C. Ummenhofer
cummenhofer@whoi.edu

[1] Tree-Ring Laboratory, Lamont-Doherty Earth Observatory, Columbia University, 61 Route 9W, Palisades, NY 10964, USA

[2] Department of Physical Oceanography, Woods Hole Oceanographic Institution, Woods Hole, MA, USA

[3] Department of History and Archaeology, University of Barcelona, Barcelona, Spain

[4] Institut Català Ciències del Clima (IC3), Barcelona, Catalonia, Spain

[5] Climate Dynamics and Landscape Evolution, German Centre for Geosciences, Potsdam, Germany

[6] Research Center Juelich Institute of Bio-and Geosciences, Agrosphere (IBG-3), Juelich, Germany

[7] Climate and Environmental Physics, University of Bern, Bern, Switzerland

[8] Department of Ecology, University of Barcelona, Barcelona, Spain

1 Introduction

Located at the westernmost edge of the Mediterranean, the Iberian Peninsula (IP) is exposed to atmospheric phenomena of Mediterranean and North Atlantic origin. Iberian hydroclimate is characterised by strong spatiotemporal variability (Fig. 1). While some eastern and southern Iberian regions are semi-arid, precipitation along the northern coast exceeds 1500 mm/year with dry summers and wet cool seasons.

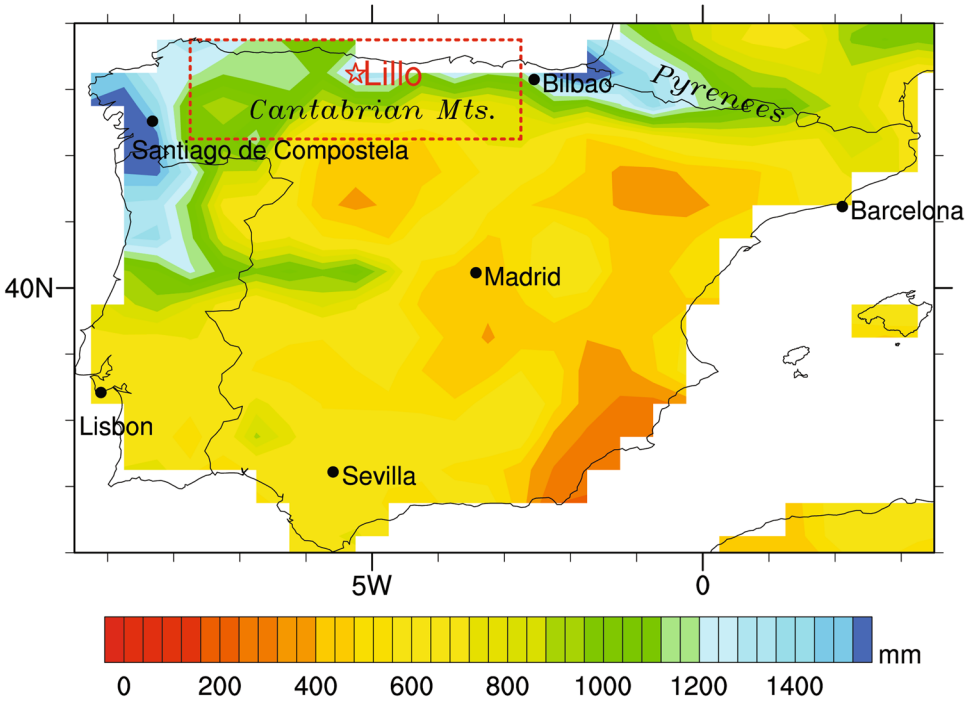

Fig. 1 Mean observed annual precipitation (mm) in the Iberian Peninsula for the period 1901–2002: The Lillo study site (*star*) and other key locations are indicated. *Red dashed box* delimits the target region used to create the Lillo precipitation and temperature time series used in this study

Despite this, drought is a familiar occurrence in the IP: analysing drought evolution during 1910–2000, Vicente-Serrano (2006) found intense and widespread drought episodes in the 1940s, 1950s, 1980s, and 1990s, with higher intensity in the central and western IP than in the northeastern region. Developing technical solutions to recurring and extended water scarcity through infrastructure building, advanced water management, and legislation has a rich and successful history over past centuries in Spain, which is still reflected today in more dams per capita than in any other country in the world (Llamas 2003). This is even more crucial considering the projected subtropical drying in a warming world due to increased subsidence across the region driven by an expansion of the Hadley cell (Lu et al. 2007, 2009; Previdi and Liepert 2007; Cai et al. 2012; Karnauskas and Ummenhofer 2014; Lau and Kim 2015), which is likely to put further strain on limited water resources in the future. The Mediterranean region has been identified as one of the top climate change hot-spots worldwide (Giorgi 2006). Recent changes in IP precipitation and temperature suggest that some of these trends towards increasing aridity are already under way (Giorgi and Lionello 2008; De Luis et al. 2009; Hoerling et al. 2012).

More frequent extremes in hydroclimate, such as floods and droughts, are likely in a warming world (Wentz et al. 2007; Trenberth 2011; Hartmann et al. 2013). Records of past hydroclimate variability thus provide an important long-term context for devising management strategies for water resources. Tree rings are natural archives that can provide information about the Earth's past environmental conditions with precise annual resolution. By applying dendrochronological techniques, it is possible to assess the relationships between trees and environmental factors and use this information to estimate climate conditions before the existence of instrumental records: i.e. generate palaeoclimatic reconstructions. The traditional tree-ring parameters are annual ring-width (TRW) and maximum density (Fritts 1976), but annually resolved isotopic chronologies based on tree rings have increased in number during the last few decades (e.g. McCarroll and Loader 2004; Seftigen et al. 2011; Gagen et al. 2012; Loader et al. 2013; Konter et al. 2014; Labuhn et al. 2014; Naulier et al. 2015; and references therein). European multi-proxy precipitation reconstructions over the last 500 years show distinct spatial, seasonal and temporal patterns, especially between central Europe and the IP, and unstable relationships between regional precipitation and large-scale atmospheric patterns (Cook et al. 2002; Pauling et al. 2006; Vicente-Serrano and López-Moreno 2008). Although drought reconstructions covering Europe (Cook et al. 2015) and specifically focused on the Mediterranean (Nicault et al. 2008) are also available, the quality of the reconstructions is not spatially homogenous, in some cases having issues over the IP. At a smaller scale, there are several temperature and precipitation reconstructions in Spain based on TRW (Fernández et al. 1996; Manrique and Fernandez-Cancio 2000; Dorado Liñán et al. 2015; Esper et al. 2015; Tejedor et al. 2015) and tree-ring density chronologies (Buntgen et al. 2008; Dorado Liñan et al. 2012). Some studies also used the stable isotopic signatures of IP tree rings

for climate related studies (Andreu-Hayles 2007; Andreu et al. 2008; Planells et al. 2009; Andreu-Hayles et al. 2011; Dorado Liñan et al. 2012, 2015; Konter et al. 2014).

Climate variability in the northwestern IP is associated with the North Atlantic Oscillation (NAO) (Rodó al. 1997; Rodriguez-Puebla et al. 1998). The NAO, defined by the pressure difference between the Azores High and the Icelandic Low, determines the strength and position of the westerly flow and thus, the main precipitation patterns across Europe, and to a lesser extent in eastern North America, and Africa (Hurrell 1995). It also impacts fish inventories, agriculture, and hydroelectric production through available water resources (Trigo et al. 2004; López-Moreno et al. 2007; Vicente-Serrano and López-Moreno 2008). Although the NAO is considered the dominant mode of interannual variability for European climate, its effect is dominant in winter, as the associated pressure changes during summer are weaker and thus exert less influence on hydroclimate variability (Trigo et al. 2008; Hernández et al. 2015). During summer, storm track activity is reduced and European hydroclimate, in particular heat extremes, are often associated with atmospheric blocking situations (Lehmann and Coumou 2015). Links to the Summer North Atlantic Oscillation (SNAO) have been made (Linderholm et al. 2009; Buwen et al. 2013). During a positive SNAO, based on an index of July–August sea level pressure (SLP) variability in the North Atlantic sector, anticyclonic conditions occur over the UK, whereas the Mediterranean area is wet and cloudier (Bladé et al. 2011).

Here, we use tree-ring samples from a *Pinus sylvestris* relict forest (García Antón et al. 1997) located at 1600 m a.s.l in the Cantabrian range near to the village '*La Puebla de Lillo*' (herein Lillo) to infer hydroclimate variability for the last 400 years in northwestern Iberia (Fig. 1). Using three different tree-ring parameters from the same chronology: TRW, carbon ($\delta^{13}C$) and oxygen ($\delta^{18}O$) stable isotopes, we applied linear and non-linear methods to determine the climatic signal recorded by these trees. Our findings include significant linkages between distinct tree-ring proxies and regional late spring and summer precipitation associated with specific atmospheric patterns.

2 Data and methods

2.1 The tree-ring chronologies

The TRW, $\delta^{13}C$ and $\delta^{18}O$ data presented here (Fig. 2) have been previously used in studies with different goals (e.g. Treydte et al. 2007; Andreu et al. 2008; Andreu-Hayles et al. 2011; Saurer et al. 2014; Frank et al. 2015). The TRW series were standardised using the residual method with a 250-year spline (Cook and Kairiukstis 1990) on power transformed series (Cook and Peters 1997). Other standardisation methods, such as the Signal Free method (Melvin and Briffa 2008) or the Friedman super smooth (Friedman 1984), were explored without leading to large differences among the resulting chronologies. In relation to the isotopic analyses, wood from four trees was pooled year by year (Leavitt and Long 1984; Dorado Liñán et al. 2011). The α-cellulose was extracted using sodium hydroxide, sodium chlorite and acetic acid (Loader et al. 1997) and was homogenised using an ultrasonic device (Laumer et al. 2009). Stable isotope ratios are expressed in the delta (δ) notation in per mil (‰) relative to the standards of the Vienna Pee Dee Belemnite (VPDB) for $\delta^{13}C$ and the Vienna Standard Mean Ocean Water (V-SMOW) for $\delta^{18}O$. $\delta^{13}C$ ratios were measured by combusting the cellulose in an elemental analyser (Fisons NA 1500 NC, Fisons Instruments, Milan, Italy) interfaced with an IRMS (Micromass Optima isotope ratio mass-spectrometer, VG Instruments, Manchester, UK) operating in continuous flow mode. Cellulose from spruce ("Fluka1", Fluka Chemika, Ord. # 22,181, Lot. # 380,099/1,20,200; $\delta^{13}C_{VPDB} = -23.03‰$) and graphite powder ("G5", 20–40 µm, purity 99.99%; $\delta^{13}C_{VPDB} = -21.16‰$) were used as laboratory standards for $\delta^{13}C$ after calibration against IAEA CH-3 (−24.7‰), IAEA-CH7 (−32.15‰) and USGS24 (−16.04‰). The $\delta^{18}O$ values were measured using high-temperature pyrolysis (1350 °C) of cellulose to carbon monoxide in a Thermo Chemical Elemental Analyser (TC/EA) coupled via a ConFlow II open split to the IRMS (Thermo Finnigan Delta Plus XL IRMS). The laboratory standards used for $\delta^{18}O$ were IAEA-C3 cellulose (32.6 ± 0.2‰), IAEA-CH6 sucrose (36.4 ± 0.2‰) and Merk cellulose (28.67 ± 0.2‰) after calibration against V-PDB and converted then to V-SMOW by using $\delta_{VSMOW} = 1.0415\ \delta_{PDB} + 41.5‰$ IAEA standards (Borella et al. 1999). The measurements' reproducibility was better than 0.1 and 0.3‰ for $\delta^{13}C$ and $\delta^{18}O$ ratios, respectively. In order to remove non-climatic trends from the raw $\delta^{13}C$ tree-ring data: we applied (1) the atmospheric correction to avoid disturbances due to the Suess effect (increase in ^{13}C-depleted atmospheric CO_2 due to fossil-fuel burning and deforestation since the industrialisation) using the values listed by McCarroll and Loader (2004); (2) the pin correction (McCarroll et al. 2009) to account for the tree ecophysiological response due to higher CO_2.

2.2 Observational/reanalysis and gridded reconstruction products

A series of monthly global gridded observational and reanalysis products were used to assess regional hydroclimate and the associated large-scale atmospheric conditions that give rise to extremes in the tree-ring proxies.

At 2.5° horizontal resolution, these include zonal and meridional winds, and specific humidity from the National

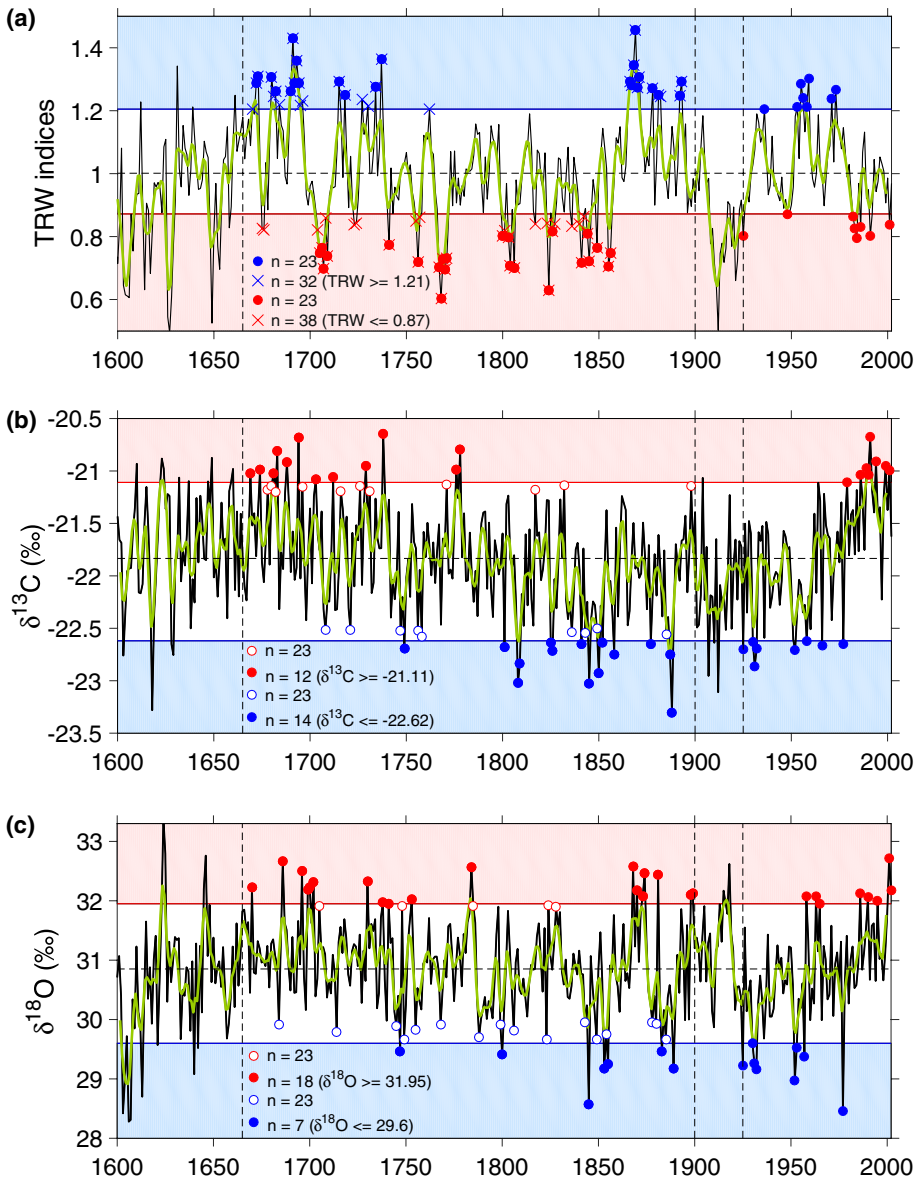

Fig. 2 Time-series of the Lillo tree-ring chronologies for the period 1600–2002 for **a** TRW, **b** $\delta^{13}C$, and **c** $\delta^{18}O$. The *circles* show the years with extreme values in the *top* and *bottom* deciles of the proxy times-series: the 8 highest and 8 lowest deciles for the period 1925–2002 (Table 1) and the 23 highest and 23 lowest values for the period 1665 to 1900 (Table 2). *Filled circles* indicate that the values are above or below the thresholds (*horizontal lines*) established in the instrumental period by the lowest of the uppermost decile and the highest of the lowermost decile of the proxy values from 1925–2002 (Table 1). Vertical dashed lines delineate the studied pre-instrumental period from 1665 to 1900 and the instrumental period from 1925 to 2002

Centers for Environmental Prediction (NCEP)/National Center for Atmospheric Research (NCAR) reanalysis (NNR; 1948–present; Kalnay et al. 1996; Kistler et al. 2001) and the 2° horizontal resolution Twentieth Century reanalysis (20CR; 1871–2011; Compo et al. 2011); precipitation at 0.5° horizontal resolution from the Global Precipitation Climatology Centre (GPCC; version 6; 1901–2010; Schneider et al. 2014) and temperature at 0.5° resolution from the Climate Research Unit (CRU TS 2.1; 1901–2002; Mitchell and Jones 2005). The common analysis period was taken as 1925–2002 (see section below), though results were repeated for the more recent period post–1957 with improved data coverage. Given the robustness of the results, we only show analyses for the longer period 1925–2002. Prior to the instrumental period, we used two 0.5° resolution gridded products: reconstructions of SLP fields from 1500 to 1999 (Luterbacher et al. 2002) and the Old World Drought Atlas (OWDA), a set of yearly maps of the reconstructed self-calibrating Palmer Drought Severity Index (scPDSI) for the summer season during the Common Era based on tree rings (Cook et al. 2015). The primary variables that we compare directly with the tree-ring proxies are temperature and precipitation at the Lillo study site (box in Fig. 1) that directly affect tree growth and physiological processes. It is not implied that trees directly record or are sensitive to SLP anomalies; rather the study aims to advance understanding of tree-ring proxy reconstructions by gaining indirect information about large-atmospheric patterns in the past by knowing how the trees respond to hydroclimatic variations.

2.3 Analysis approach

The calibration period overlapping between the proxies and instrumental data was from 1925 to 2002, after excluding the beginning of the twentieth century due to continuous extreme low values observed in the TRW chronology. The persistence and magnitude of this disturbance pattern over more than two decades suggest a non-climatic origin. Most of the sampled trees had scars produced by the extraction of torches, an activity that is documented to have occurred in the studied forest from the end of the nineteenth century to the first quarter of the twentieth century (Orden Martn 2013). The same analyses performed over the entire possible calibration period (1901–2002) show consistent results with the ones presented here, although some lower climatic sensitivity in some of the proxies was observed (results not shown). The time span used for the pre-instrumental or historical period from 1665 to 1900 was determined by the reliable time-span of the TRW chronology starting in 1663 that was assessed by an Expressed Population Signal statistic higher than 0.85 (Wigley et al. 1984).

Time-series of climate data for the Lillo region were created as area-average for the domain delimited by the red box (42.25–43.75 °N; 2.75–7.75 °W) shown in Fig. 1, based on the GPCC precipitation (Schneider et al. 2014) and the CRU temperature (Mitchell and Jones 2005) gridded data sets. The initial identification of monthly and seasonal climate signals in the tree-ring data was assessed through correlations of the three tree-ring chronologies with precipitation, as well as partial correlations with mean temperature data controlling the influence of precipitation using the approach implemented in Seascorr (Meko et al. 2011).

An analysis of extremes was used to (1) provide insights on the physiological processes affecting the tree-ring proxies (box plot analyses); (2) to accommodate non-linear tree-ring responses to variations in hydroclimate with regard to the sign of the anomaly and its seasonality (seasonal cycles); (3) to understand the seasonal large-scale atmospheric mechanisms associated with these years (composite maps). As is customary for non-normally distributed variables, such as precipitation, all values in the three tree-ring proxy time-series were ranked and the lowest/highest decile (i.e. extremes) were selected. This led to a selection of 8 high and 8 low extreme years for the instrumental period 1925–2002 (Table 1) and a total of 23 high and 23 low extreme years for the historical period 1665–1900 (Table 2) comprising 236 years. Proxy values for the extreme years were compared using box-and-whisker plots. We assessed the characteristics of the seasonal cycle of Lillo precipitation and surface air temperature (SAT) during these 8 years with extreme high (low) proxy values for the instrumental period, with the coloured lines indicating the mean seasonal cycle for the three parameters. To determine whether the mean seasonal cycle during these extreme years differs significantly from average years a boot-strapping method (i.e. Monte Carlo test) was employed: for a particular time-series, 8 random years were selected for the period 1925–2002. This was repeated 25,000 times to generate an expected distribution of the seasonal cycle for any given set of 8 years. The grey shading represents the 90% significance level of this expected distribution for high (low) years. Wherever a coloured line lies outside the grey shading, the precipitation or SAT in the extreme years differs significantly from average conditions.

Using those same years, composite anomalies of precipitation, SAT, moisture transport, and SLP were calculated for those months when the seasonal precipitation cycle during extreme years deviates significantly from average rainfall conditions based on all years. A two-tailed *t* test was used to determine whether composite anomalies of precipitation, SAT, moisture transport, and SLP were significant at the 90% level from the long-term mean based on all years.

The years with extreme values in the palaeo proxy time-series (TRW, $\delta^{13}C$, and $\delta^{18}O$) for the previous centuries

Table 1 Years with extreme values in the top and bottom deciles (10%): the ranked 8 highest and 8 lowest values for the time-series of the Lillo tree-ring chronologies for the period 1925–2002 for (left) TRW, (middle) $\delta^{13}C$, and (right) $\delta^{18}O$

Wet years					
Year	High TRW	Year	Low $\delta^{13}C$	Year	Low $\delta^{18}O$
1959	1.30	1958*	−22.62*	**1930***	29.60*
1955	1.29	**1930**	−22.63	1953	29.53
1973	1.27	**1977**	−22.65	1957	29.38
1956	1.24	1966	−22.66	**1931**	29.26
1971	1.24	**1932**	−22.69	**1925**	29.22
1958	1.21	**1925**	−22.70	**1932**	29.16
1953	1.21	**1952**	−22.71	**1952**	28.97
1936*	1.21*	**1931**	−22.86	**1977**	28.46
Dry years					
Year	Low TRW	Year	High $\delta^{13}C$	Year	High $\delta^{18}O$
1948*	0.87*	1991	−20.67	**2001**	32.71
1982	0.86	1994	−20.91	2002	32.18
2001	0.84	1999	−20.95	**1986**	32.12
1986	0.83	1989	−20.97	1958	32.08
1983	0.83	**2001**	−20.99	1963	32.08
1925	0.80	**1986**	−21.04	**1990**	32.06
1991	0.80	**1990**	−21.04	1995	32.00
1984	0.79	1979*	−21.11*	1965*	31.95*

The years in agreeement between $\delta^{13}C$ and $\delta^{18}O$ are indicated in bold

The years with the lowest of the uppermost decile and the highest of the lowermost decile of the proxy values are indicated with * and were used as thresholds for analyses in the pre-instrumental period

Table 2 Years with extreme values in the top and bottom deciles (10%): the 23 highest and 23 lowest values for the time-series of the Lillo tree-ring chronologies for the period 1665–1900 for (left) TRW, (middle) $\delta^{13}C$, and (right) $\delta^{18}O$

(a) Years with extreme values within the top/bottom decile range (10 %) from 1665 to 1900

Wet years			Dry years		
High TRW	Low $\delta^{13}C$	Low $\delta^{18}O$	Low TRW	High $\delta^{13}C$	High $\delta^{18}O$
1672	1708	1684	**1705**	**1669**	**1670**
1673	1721	1714	**1706**	**1674**	**1686**
1680	1747	1745	**1707**	1678	**1696**
1682	**1749**	**1747**	**1709**	1680	**1699**
1690	1756	1749	**1741**	**1681**	**1700**
1691	1758	1755	**1756**	1682	**1702**
1692	**1801**	1768	**1767**	**1683**	1705
1693	**1808**	1788	**1768**	**1688**	**1730**
1694	**1809**	1799	**1769**	**1694**	**1738**
1715	**1825**	**1800**	**1770**	1696	**1741**
1718	**1826**	1806	**1771**	**1703**	1748
1734	1836	1823	**1800**	**1712**	**1753**
1737	**1841**	1843	**1803**	1716	**1784**
1866	1843	**1845**	**1804**	1726	1785
1867	**1845**	1849	**1806**	**1729**	1824
1868	1849	**1853**	**1824**	1731	1828
1869	**1850**	1854	**1826**	**1738**	**1868**
1870	**1852**	**1855**	**1841**	1771	**1870**
1871	**1858**	1878	**1844**	**1776**	**1873**
1878	**1877**	1880	**1845**	**1778**	**1874**
1881	1885	**1883**	**1849**	1817	**1881**
1892	**1887**	1885	**1855**	1832	**1898**
1893	**1888**	**1889**	**1856**	1898	**1899**

(b) Years with extreme values outside the top/bottom decile range (10 %) from 1665 to 1900

Wet years	Dry years
High TRW	Low TRW
1670, 1681, 1684	1675, 1676, 1704
1695, 1696, 1727	1708, 1723, 1724
1730, 1762, 1882	1755, 1757, 1801
	1817, 1823, 1827
	1836, 1840, 1842

Years with proxy values above or below the thresholds (horizontal lines in Fig. 2) established in the instrumental period (1925–2002) by the lowest of the uppermost decile and the highest of the lowermost decile of the proxy values (Table 1) are indicated: (a) bold values: when those years overlapped with the 23 years within the deciles; (b) listed at the end just for TRW: when those years are in addition to the 23 years within the deciles

were detected by two distinct approaches (Table 2): (a) *decile method*: 23 high/low extreme proxy years detected as deciles for the period 1665–1900 (Fig. 2, circles); (b) *threshold method*: years with proxy values that exceeded a threshold value determined by the lowest of the uppermost decile and the highest of the lowermost decile of the proxy values in the instrumental period 1925–2002 (Table 1; horizontal red/blue line in Fig. 2). For those high/low extreme proxy years detected by the threshold method throughout the historical period (1665–1900), composite anomalies were calculated for SLP reconstructed fields over the eastern North Atlantic region and Europe (Luterbacher et al. 2002) and for scPDSI based on the OWDA (Cook et al. 2015). Composites were also calculated for the 8 high/low extreme years for the instrumental period for validating the method for SLP and scPDSI. Finally, the number of occurrence of years with extreme events per decade obtained in 20-year sliding windows for the two isotope proxies was calculated. The temporal evolution of extreme events is only shown for the sign, for which strong significant deviations in the seasonal cycle of Lillo precipitation were detected based on the seasonal cycle analyses.

3 Distinct climatic signals in the tree-ring proxies

The climatic signal recorded by each tree-ring proxy (TRW, $\delta^{13}C$ and $\delta^{18}O$) show distinct strength and seasonality (Fig. 3). Tree growth, represented by TRW records, is mildly favoured by wet conditions from April to July (i.e. positive correlation between TRW and precipitation); in contrast the effect of temperature, with the precipitation effect removed, seems to be negligible without a single month with significant correlation. The tree-ring parameter most sensitive to summertime water availability is $\delta^{13}C$. The $\delta^{13}C$ records exhibit the highest climate sensitivity with significant negative correlation with June–July precipitation and positive partial correlation with July–August temperatures. The $\delta^{18}O$ records exhibit weaker correlations, but similar seasonal sensitivity to $\delta^{13}C$ with negative and positive correlations from May to July precipitation and July to September temperatures, respectively (Fig. 3). Therefore, both stable isotopic ratios ($\delta^{13}C$ and $\delta^{18}O$) seem to be mainly modulated by changes in moisture during summertime.

4 Physiological processes related to climate variability

There are constant fractionation processes affecting the $\delta^{13}C$ signatures due to CO_2 diffusion through stomata and carboxylation (by Rubisco during photosynthesis), but other fractionations can also occur due to changes in environmental conditions. These are the signals sought in this paper. The $\delta^{13}C$ ratios may be lower (ratios depleted in the heavier isotope ^{13}C) during wet summers because

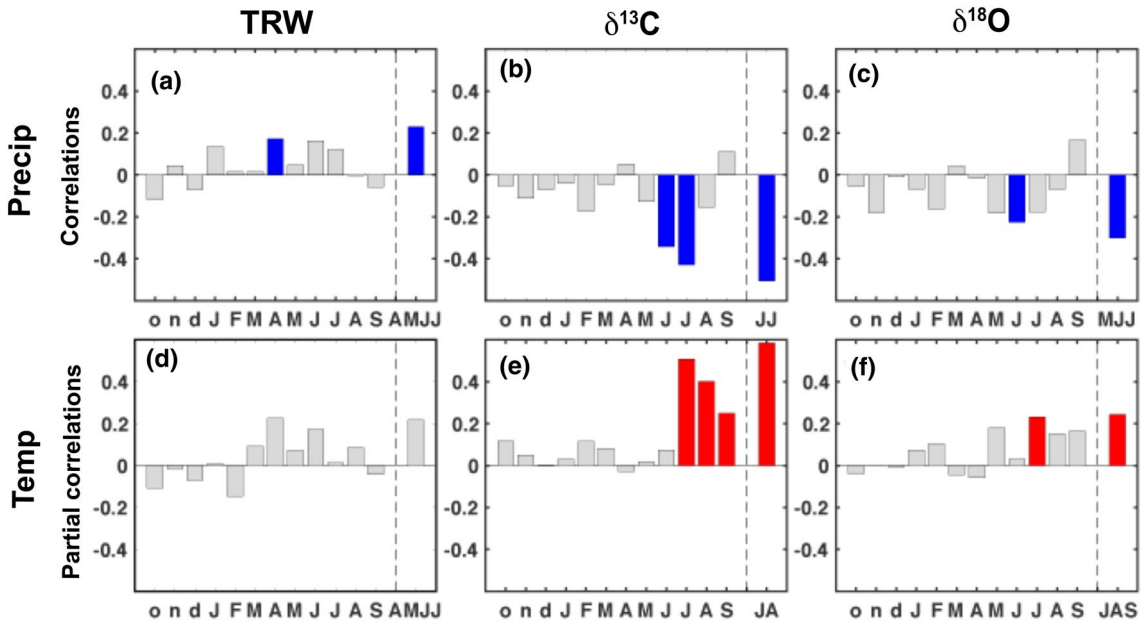

Fig. 3 Correlations for monthly precipitation and partial correlations for monthly temperature, from October in the previous year to September of the current year for the period 1925–2002 with tree-ring parameters for (*left*) TRW, (*middle*) $\delta^{13}C$, and (*right*) $\delta^{18}O$. *Coloured bars* indicate significant correlation coefficients at the 95% confidence level

more open stomata lead to more CO_2 available in the stomatal chambers. This leads to more discrimination against the heavier isotope, ^{13}C, since the lighter isotope, ^{12}C, is preferred as a substrate for photosynthesis (Farquhar et al. 1982). Dry summers may lead to higher $\delta^{13}C$ values (ratios enriched in ^{13}C) since closed stomata allow less CO_2 availability in the stomatal chambers, and thus discrimination against ^{13}C is lower. However, an enrichment (depletion) of the $\delta^{13}C$ isotopic signature due to higher (lower) assimilation rates linked to temperature or light influences on photosynthesis (McCarroll and Pawellek 1998) cannot be initially ruled out. Both physiological processes, assimilation increase (decrease) and stomata conductance decrease (increase) produce the same isotopic signature as a result of reducing (increasing) the ^{12}C availability in the stomatal chambers. However, our results show significantly lower and higher $\delta^{13}C$ ratios during the years with the 8 highest and 8 lowest growth observed (Fig. 4a), respectively. This suggests a stronger regulation by stomatal variations (e.g. close stomata may lead to higher $\delta^{13}C$ and lower TRW) and not by changes in assimilation (e.g. more photosynthesis may lead to higher $\delta^{13}C$ and higher TRW).

The $\delta^{18}O$ values are mainly affected by the original values of the $\delta^{18}O$ of the source water and the fractionation processes at the leaf level through stomatal conductance (Barbour 2007), same as the mechanism explained above for $\delta^{13}C$. This leads to lower $\delta^{18}O$ ratios (depleted in heavy isotopes, ^{18}O) during wet summers and to higher $\delta^{18}O$ ratios (enriched in ^{18}O) during dry summers. In UK, for instance, during cyclonic wet summers, $\delta^{18}O$ ratios in cellulose are lower because of low $\delta^{18}O$ values in rainfall (source water) and a lowered evaporative enrichment process at the leaf level due to lower vapour pressure due to moist air (Young et al. 2015). In contrast during anticyclonic conditions, the opposite fractionation processes occur.

Temperatures may also have an independent effect supported by the significant partial correlations with both stable isotopic series after removing the influence of precipitation (Fig. 3e, f). Warm and cold summers may enhance the enrichment (high) and depletion (low) of isotopic ratios, respectively, via changes in vapour pressure at leaf level through stomata conductance. In summary, higher $\delta^{13}C$ and $\delta^{18}O$ values (~enriched) document drier and warmer conditions, whereas lower $\delta^{13}C$ and $\delta^{18}O$ values (~depleted) are related to wetter and colder conditions.

The years detected by the $\delta^{13}C$ and $\delta^{18}O$ extreme values do not always coincide with 6 out of 8 and 3 out of 8 matches for wet years and dry years, respectively (Table 1). Despite this, the box plot analyses (Fig. 4) confirm the coherence between both proxies. During the 8 years with the highest/lowest $\delta^{13}C$ ratios (Fig. 4e), the $\delta^{18}O$ values were significantly higher and lower, respectively. Likewise during years with the 8 highest/lowest $\delta^{18}O$ ratios (Fig. 4f), the $\delta^{13}C$ ratios were significantly higher and lower, respectively. A correlation value of 0.58 between the $\delta^{13}C$ and $\delta^{18}O$ records supports that summer moisture availability is regulating both isotopes at the leaf level. Nevertheless, other environmental factors are also independently

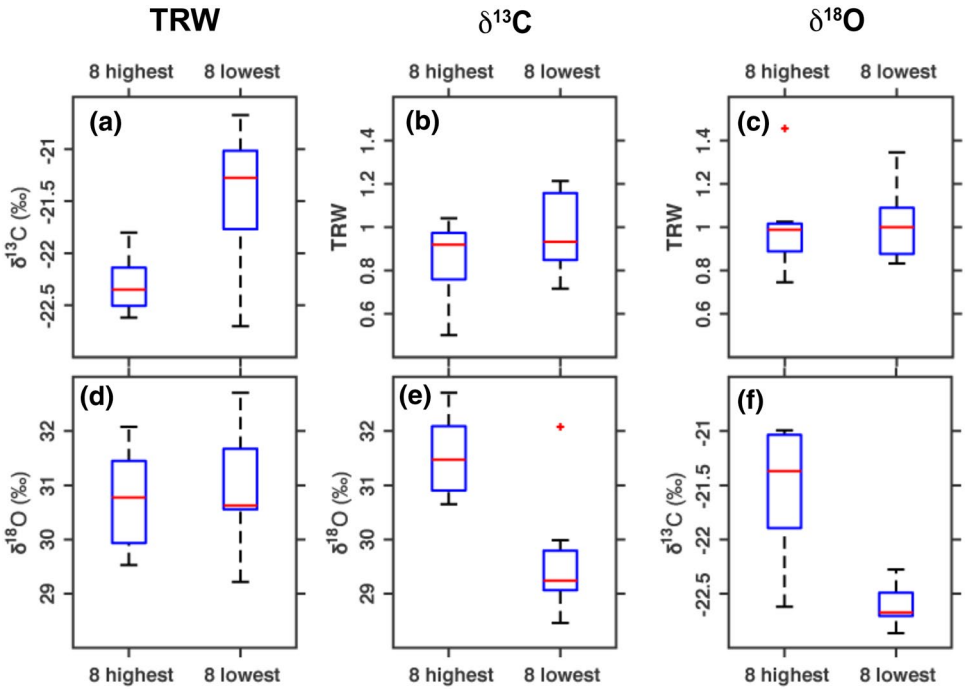

Fig. 4 Box-and-whisker plots for the values of the tree-ring records during the 8 years of extreme high/low values for each tree-ring record: (*left*) TRW, (*middle*) $\delta^{13}C$ and (*right*) $\delta^{18}O$. The *red line* represents the median, the *blue boxes* delimit the 25th and 75th percentile (i.e. interquartile range) and whiskers the minimum and maximum values

modulating each proxy. The lower climatic sensitivity of $\delta^{18}O$ compared to $\delta^{13}C$ records may be partially due to the contribution of the original values of the source water (Saurer et al. 2002) and fractionation processes occurring in this meteoric water until the fixation of the $\delta^{18}O$ in plant tissue (McCarroll and Loader 2004).

5 Asymmetric moisture signal in high and low extreme proxy years

Figure 5 shows the tree-ring series and seasonal cycle for precipitation and temperature for the study site Lillo (red box in Fig. 1) for the instrumental period 1925–2002. Years recording the highest/lowest 10% of the values in each tree-ring record (i.e. deciles) were selected [blue/red filled circles in Fig. 5 for (a) TRW, (b) $\delta^{13}C$, and (c) $\delta^{18}O$], and used to calculate the seasonal cycle in precipitation (d, f) and temperature (g, i). Blue lines illustrate the seasonal cycle for years with high precipitation detected by wide (high) TRW, depleted (low) $\delta^{13}C$ and depleted (low) $\delta^{18}O$ values. Red lines show the seasonal cycle for years with low precipitation detected by narrow (low) TRW, enriched (high) $\delta^{13}C$ and enriched (high) $\delta^{18}O$. Therefore, significantly wetter conditions than average (blue lines outside the grey band) are detected in June by extreme wide TRW values and in June–July by extreme low $\delta^{13}C$ and $\delta^{18}O$ ratios. In contrast, significantly drier conditions (red lines outside the grey band) are detected in June associated with the narrowest TRW and the highest $\delta^{13}C$, and in May related to extreme high $\delta^{18}O$ ratios.

For the temperature seasonal cycles (g–i), blue lines indicate that these years exhibit low temperatures in July–August detected by depleted (low) $\delta^{13}C$ and in July by depleted (low) $\delta^{18}O$. Red lines indicate warm conditions in July and August for years with enriched (high) $\delta^{13}C$. Extreme wide TRW are significantly related to warm temperatures in April–May that may favour the onset of the growing season, while narrow TRW seem to be associated, with colder temperatures during those months.

These seasonal cycle analyses indicate that months with significant deviations from average climatic conditions differ between years with extreme high and low proxy values. Thus, timing (years and seasons) of climatic extremes is different for high and low extremes of the same proxy. For instance, in years with extreme high $\delta^{13}C$ values (Fig. 5b) significantly drier conditions occurred during June, but the wetter conditions detected by the low $\delta^{13}C$ value occurred during July–August (Fig. 5e). Overall, climatic sensitivity is seasonally shifted between proxy high/low values: dry conditions are detected to occur earlier in the year in late spring, while wet conditions are found to occur later during the summer months.

6 Atmospheric patterns associated with wet/dry conditions

The months identified by the precipitation seasonal cycle analysis with significant deviations in precipitation from mean conditions are consistent with large-scale atmospheric

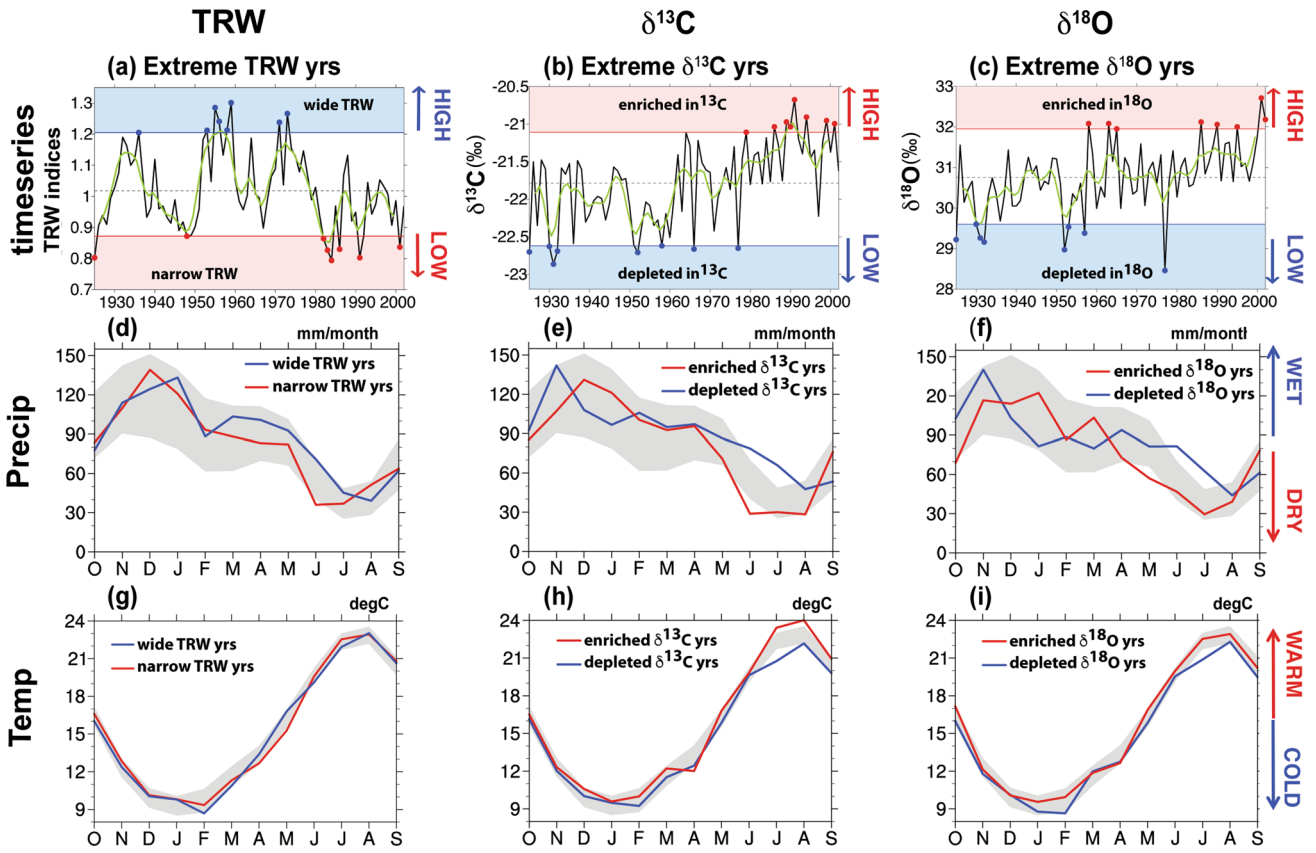

Fig. 5 Lillo tree-ring series and seasonal cycles for precipitation and temperature: **a–c** Time-series of tree-ring chronologies for the period 1925–2002 for (*left*) TRW, (*middle*) $\delta^{13}C$, and (*right*) $\delta^{18}O$. Annual values are shown in *black*, 5-year moving average in *green*, and years with extreme high and low values in the time-series highlighted with *filled circles*. **d–i** Average seasonal cycle (*grey shading*) and seasonal cycles during years with the extreme proxy values detected in **a–c** shown with *coloured lines* for **d–f** Lillo precipitation and **g–i** Lillo temperature. Where the *coloured lines* lie outside the *grey shading*, significant deviations from average conditions occur

features described by composite analyses for the same months (Figs. 6, 7). Our composite anomaly maps indicate different circulations patterns for high and low extreme years. It should be noted that the composites show anomalies rather than the mean field, so the circulation changes thus relate more to a strengthening or weakening of the westerly onshore moisture transport for example, rather than a complete change in direction and therefore change in source water region.

6.1 Wet summer conditions

The seasonal temperature and precipitation cycles in years with extreme low $\delta^{13}C$ values (Fig. 5b) show significantly colder conditions for July (Fig. 5h) and wetter conditions during June–July (Fig. 5e), respectively. The June–July composites for years with extreme low $\delta^{13}C$ show significantly wetter and colder conditions for the Cantabrian range, western Iberia and southwestern France (Fig. 6b, e). This is associated with an enhanced onshore moisture transport from the Atlantic Ocean (Fig. 6h) driven by significant positive SLP anomalies at high latitudes and negative anomalies over Europe (Fig. 6k). Similar patterns are found during years with low $\delta^{18}O$ values (Fig. 5c) with significant anomalies in the precipitation and temperature seasonal cycles detected, corresponding to wetter (Fig. 5f) and colder (Fig. 5i) early summer conditions. Composite anomalies for these years during June–July confirm significantly higher precipitation over the northern IP and southern France (Fig. 6c), enhanced moisture transport from the Atlantic (Fig. 6i) and consistent SLP patterns (Fig. 6l), with significantly colder conditions across the IP (Fig. 6f). The composites corresponding to years with wide TRW values associated with anomalous wet conditions for June in the seasonal cycle (Fig. 5d) show higher precipitation along the northern IP (Fig. 6a), associated with coherent moisture transport (Fig. 6g) and SLP patterns (Fig. 6j), as well as colder temperatures over the IP (Fig. 6d). The moisture transport in years with high TRW values shows more local atmospheric features with moisture coming directly from the west (Fig. 6g), resulting in local precipitation events at the study site (Fig. 6a). In contrast, moisture transport patterns associated with the low isotopic values (Fig. 6h, i)

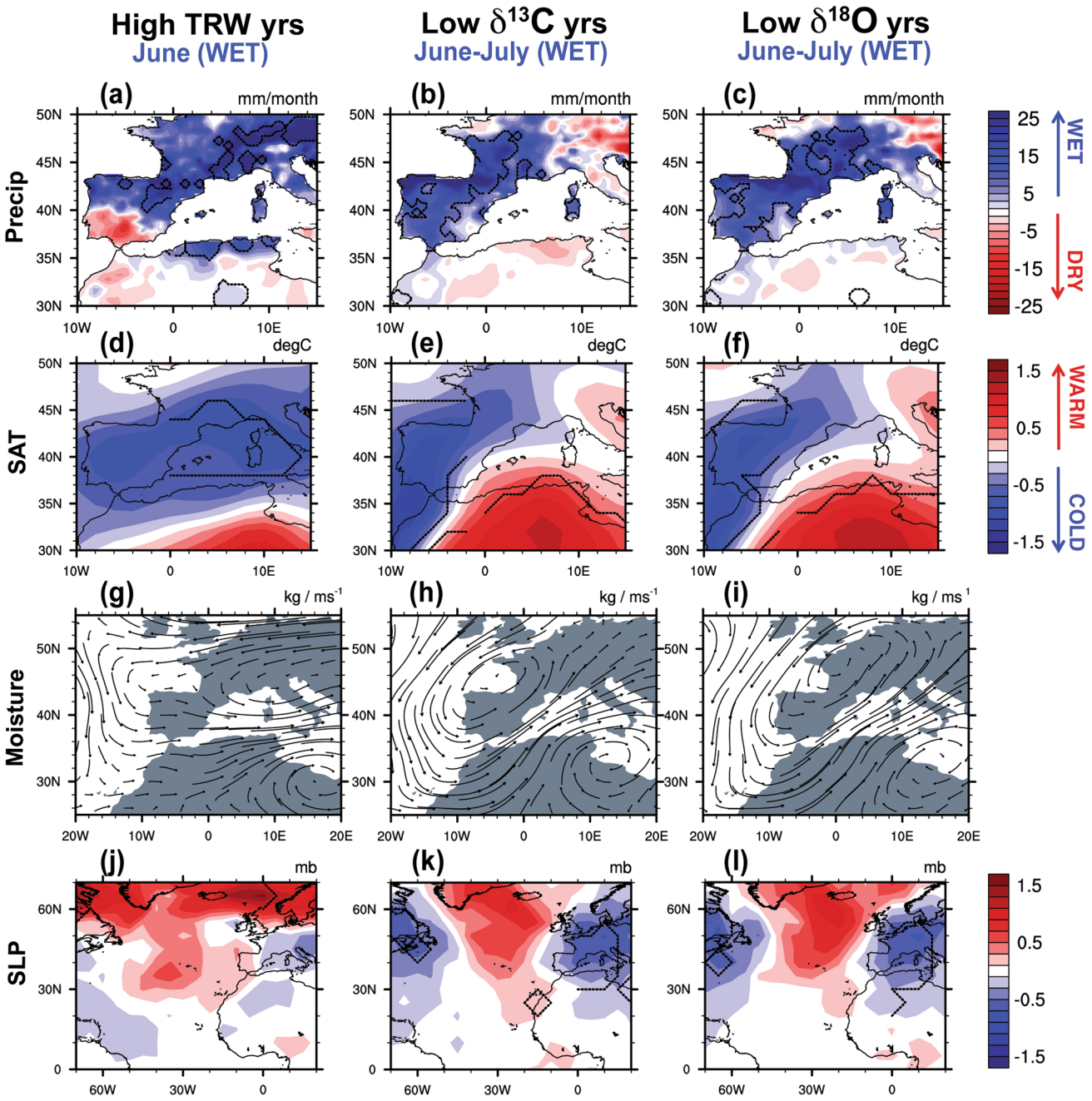

Fig. 6 Composites of wet summer conditions during years with extreme values in the tree-ring series in the studied instrumental period (1925–2002). Note that wet conditions correspond to wide (high) values in TRW and low values for both stable isotopic ratios ($\delta^{13}C$ and $\delta^{18}O$). **a–l** Seasonal composite anomalies for years with extreme proxy values are shown for those months with significant deviations in the precipitation seasonal cycle (Fig. 5d–f) for **a–c** precipitation, **d–f** surface air temperature (SAT), **g–i** moisture transport integrated below 500 hPa, and **j–l** sea level pressure (SLP). *Dashed contours* indicate anomalies significant at the 90% confidence level

exhibit more broad-scale anomalous moisture transport features spanning across western Europe and western North Africa that lead to anomalous precipitation over a larger region of the IP and into southern France (Fig. 6b, c). These large-scale patterns detected by extreme isotopic values are associated with anomalous high SLP anomalies over Iceland and low SLP anomalies over Europe (Fig. 6k, l).

6.2 Dry late spring–early summer conditions

In years with extreme high $\delta^{13}C$ values (Fig. 5b) significantly drier conditions occurred during June (Fig. 5e) and warmer conditions during July–August (Fig. 5h). In agreement, composite anomaly maps for June for high $\delta^{13}C$ years indicate significant reductions in precipitation over

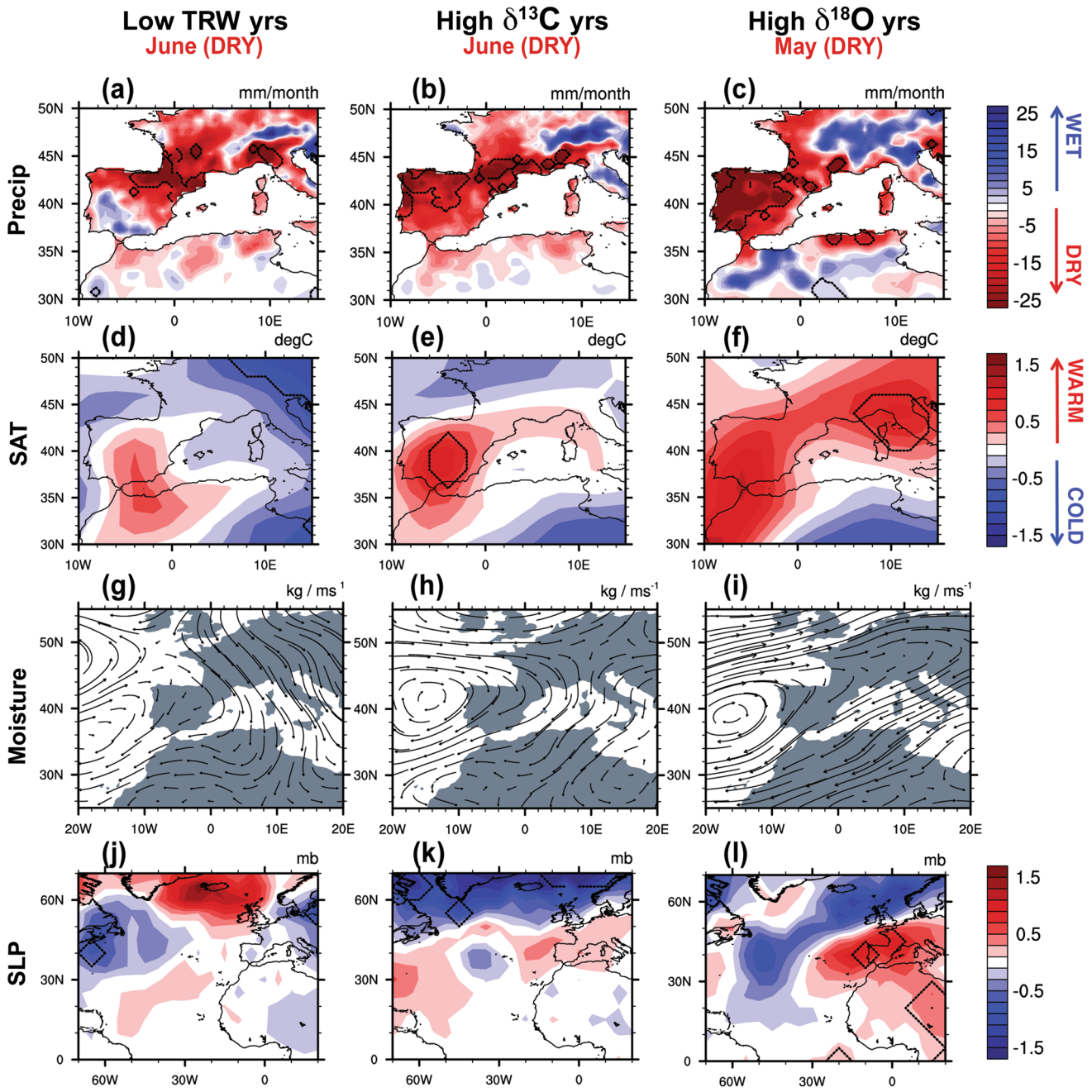

Fig. 7 Composites of dry summer conditions during years with extreme values in the tree-ring series for the studied instrumental period (1925–2002). Note that dry conditions correspond to narrow (low) values in TRW and high values for both stable isotopic ratios ($\delta^{13}C$ and $\delta^{18}O$). **a–l** Seasonal composite anomalies for years with extreme proxy values are shown for those months with significant deviations in the precipitation seasonal cycle (Fig. 5d–f) for **a–c** precipitation, **d–f** surface air temperature (SAT), **g–i** moisture transport integrated below 500 hPa, and **j–l** sea level pressure (SLP). *Dashed contours* indicate anomalies significant at the 90% level

the northwestern IP (Fig. 7b) and positive temperature anomalies over the IP (Fig. 7e), associated with coherent large-scale atmospheric circulation patterns. Anomalously low SLP over Iceland and Greenland and high SLP anomalies over western and southern Europe (Fig. 7k) result in a reduced moisture transport into the IP (Fig. 7h). In years with extreme high $\delta^{18}O$ values significantly drier conditions occur in May (Fig. 5f). Accordingly, the associated composite maps for May reveal significant reductions in precipitation over the western IP (Fig. 7c) and positive SAT anomalies across the wider IP and into France (Fig. 7f), associated with coherent large-scale atmospheric circulation

patterns. Anomalously low SLP over the North Atlantic and high SLP over Europe (Fig. 7l) result in a reduced moisture transport into the IP (Fig. 7i). While moisture transport composites for high isotopic years (Fig. 7h, i) share again very similar transport patterns, moisture advection detected by low TRW values (Fig. 7g) indicates a particular circulation pattern associated with positive anomalies over Iceland (Fig. 7j), warmer conditions over the central and southern IP (Fig. 7d) and drier conditions over the Pyrenees, but not over Lillo where the trees are located (Fig. 7a).

7 Hydroclimate in the pre-instrumental period

Seasonal composites computed for the period 1665–1900 using the SLP gridded product (Luterbacher et al. 2002) and the OWDA (Cook et al. 2015) corroborated the detection of wet/dry years in the pre-instrumental period. Table 2 shows the extreme years detected using the two approaches (decile and threshold method). The composite analyses using years from both approaches led to similar results. Thus, herein we just show results derived from the threshold method.

The SLP composites computed using years with high TRW (Fig. 8a), low $\delta^{13}C$ (Fig. 8b) and low $\delta^{18}O$ (Fig. 8c) represent SLP patterns that are consistent with wet conditions in the IP. In contrast, low TRW (Fig. 8d), high $\delta^{13}C$ (Fig. 8e) and high $\delta^{18}O$ (Fig. 8f) show SLP patterns mostly associated with dry conditions over the IP. Overall, pre-instrumental SLP composites (Fig. 8) compare well with SLP instrumental observations (Figs. 6, 7, 10), mainly showing low and high pressure anomalies over Europe during wet and dry events, respectively. More specifically, the anomalies in the pre-instrumental period resemble the SLP patterns seen during extreme wet summer months well (Figs. 8a–c, 10a–c), while there is less agreement for the dry extremes (Fig. 8d–f, 10d–f). For the latter, the SLP anomalies over central and southern Europe are consistent between the instrumental and pre-instrumental period, while it is the sign and location of maximum SLP anomalies over northern Europe that differ. The OWDA composites (Fig. 9) indicate mainly wet

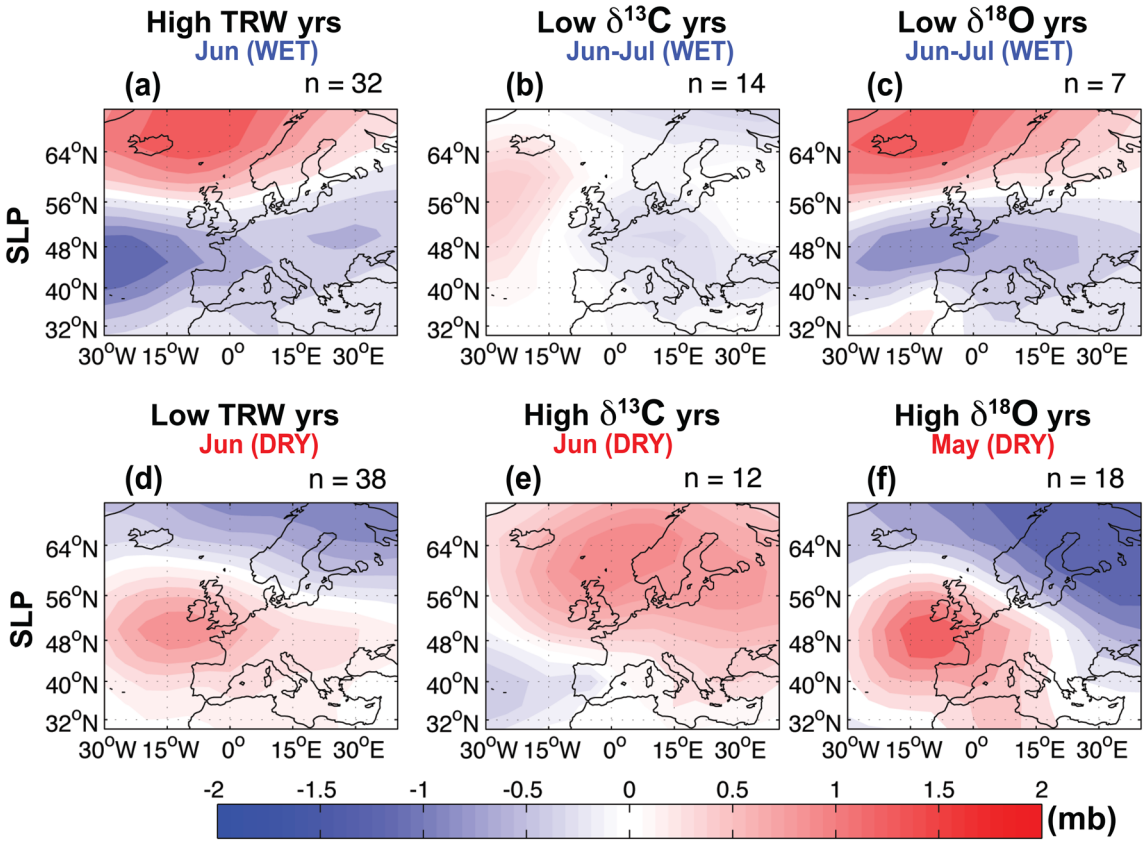

Fig. 8 Seasonal composite analyses of SLP (mb) during years with extreme values in the tree-ring series for the pre-instrumental period (1665–1900). Note that wet conditions over the Lillo site correspond to wide (high) values in TRW (**a**) and low values for both stable isotopic ratios $\delta^{13}C$ (**b**) and $\delta^{18}O$ (**c**); dry conditions to narrow (low) values in TRW (**d**) and high values for both stable isotopic ratios $\delta^{13}C$ (**e**) and $\delta^{18}O$ (**f**). *n* indicates the number of extreme years used in each composite that was based on the criteria to select years above and below the threshold established in Fig. 2

conditions (Fig. 9a–c) for years with high TRW and low isotopic ratios, whereas non-significant or slightly dry conditions occur over the Lillo area (Fig. 9d–f) for years with low TRW and high isotopic ratios. In addition, SLP (1925–1999; Fig. 10) and OWDA (1925–2002; Fig. 11) composites for the instrumental period also show consistent results with the expected dry and wet years depending on low/high extreme values detected in the tree-ring proxies. Therefore, these composites corroborate the validity of our approach of using extreme analyses in tree-ring records to explore the occurrence of wet and dry periods prior to the instrumental period.

The three tree-ring parameters present distinct sensitivity to summer moisture availability, while high and low extremes exhibit distinct seasonality and an asymmetric moisture signal. Whereas TRW seems to reflect local atmospheric circulation features, stable isotopes share some large-scale atmospheric patterns across the IP and western Europe that are of interest for this study in order to infer changes in water availability over the IP more broadly. Here, we propose a novel non-linear method to explore past hydroclimatic variability based on the analysis of extremes in the isotopic series to detect specific years in the past (Table 2), in which the proxies recorded significant deviations from average hydroclimatic conditions. Thus, the most likely occurrence of years with wet/dry conditions is recorded independently by each tree-ring parameter for the last 400 years, allowing for precise seasonality and attribution to related atmospheric patterns. Specifically, the extreme isotopic values respond to summertime/late spring moisture availability: wet June–July (low $\delta^{13}C$ and low $\delta^{18}O$), dry June (high $\delta^{13}C$) and dry May (high $\delta^{18}O$). Hence, these isotopic records are used as proxies for inferring northwestern IP hydroclimate variability during late spring/early summer during the period 1665–1900 (Fig. 12).

A consistent wet period in the second half of the nineteenth century is the most prominent feature of the reconstruction of wet summers (Fig. 12a) based on the high occurrence of wet years detected by low values in the isotopic proxies (Table 2). This is reflected in low $\delta^{13}C$ values for an extended period of time and even more pronounced in low $\delta^{18}O$ centred around 1850. Undoubtedly, indicators of 'wetness' (depleted isotope values), agree on the persistent mid-nineteenth century pluvial. In addition, any 'dryness' indicators (enriched isotope values) are absent during that period as shown in the reconstruction of dry late spring–early summer (Fig. 12b).

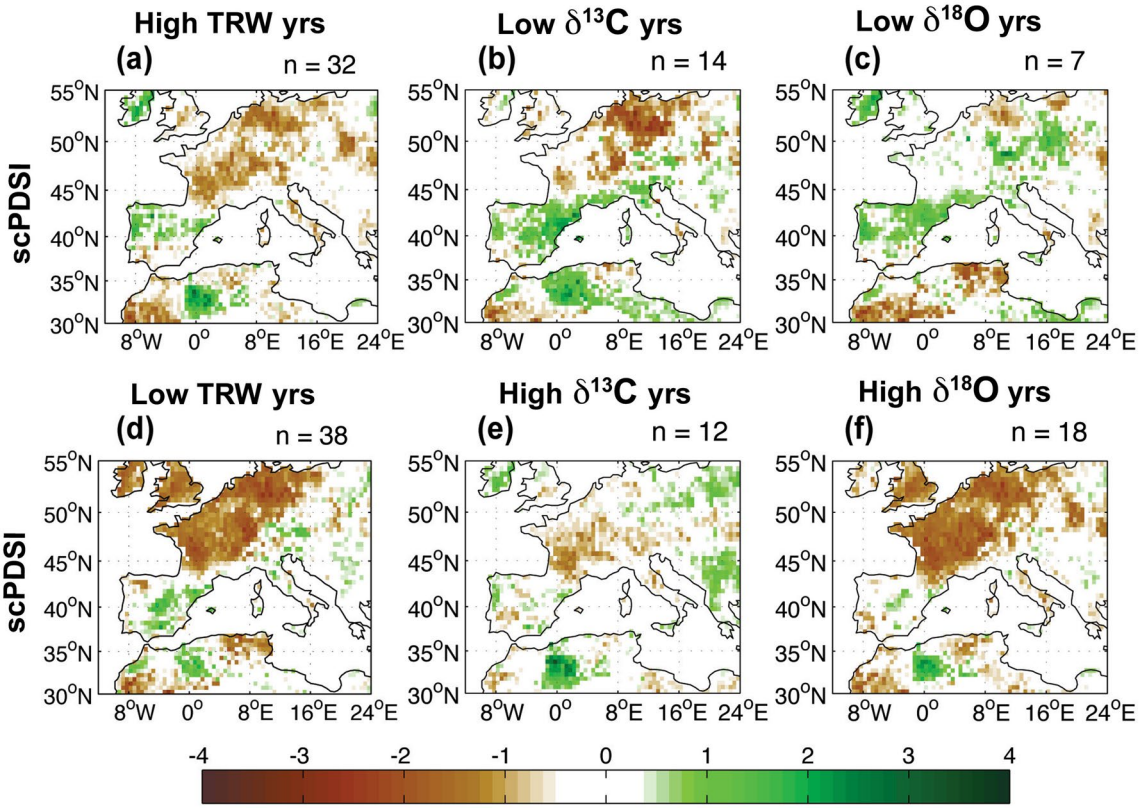

Fig. 9 As Fig. 8, but for the self-calibrating Palmer Drought Severity Index (scPDSI) from the Old World Drought Atlas (OWDA)

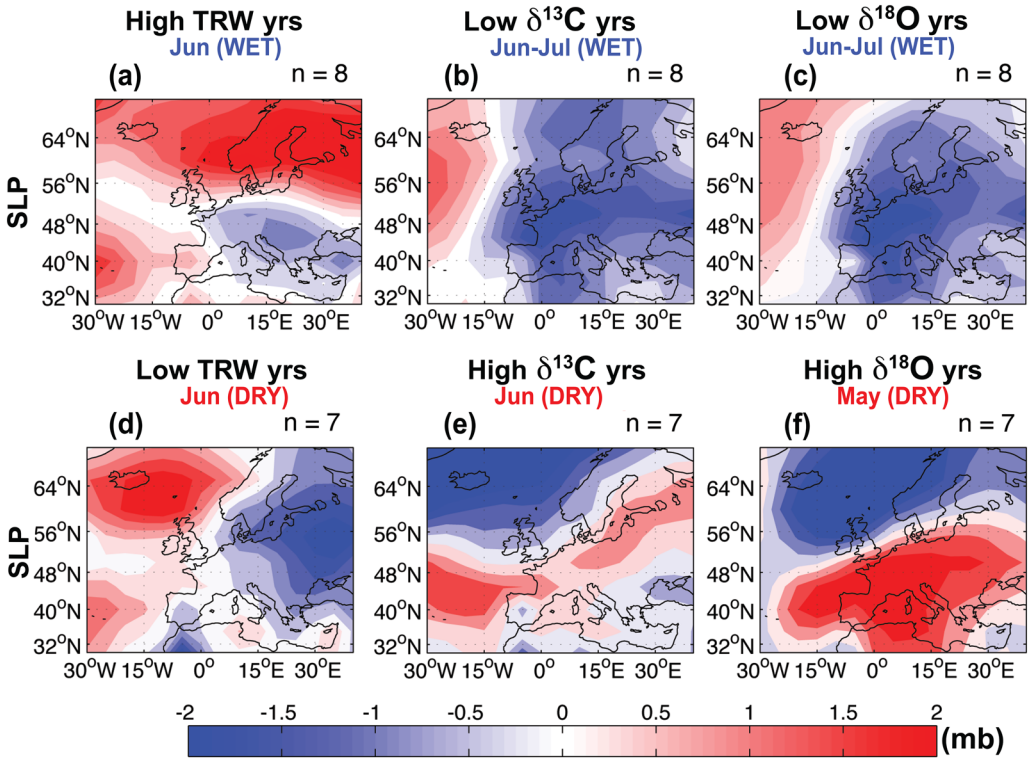

Fig. 10 As Fig. 8, but using the years detected by the 8 high/low proxy values for the instrumental period (1925–1999) for the SLP anomaly composites. Note that 7 years were used instead of 8 when the year 2001 was not available in the SLP gridded product

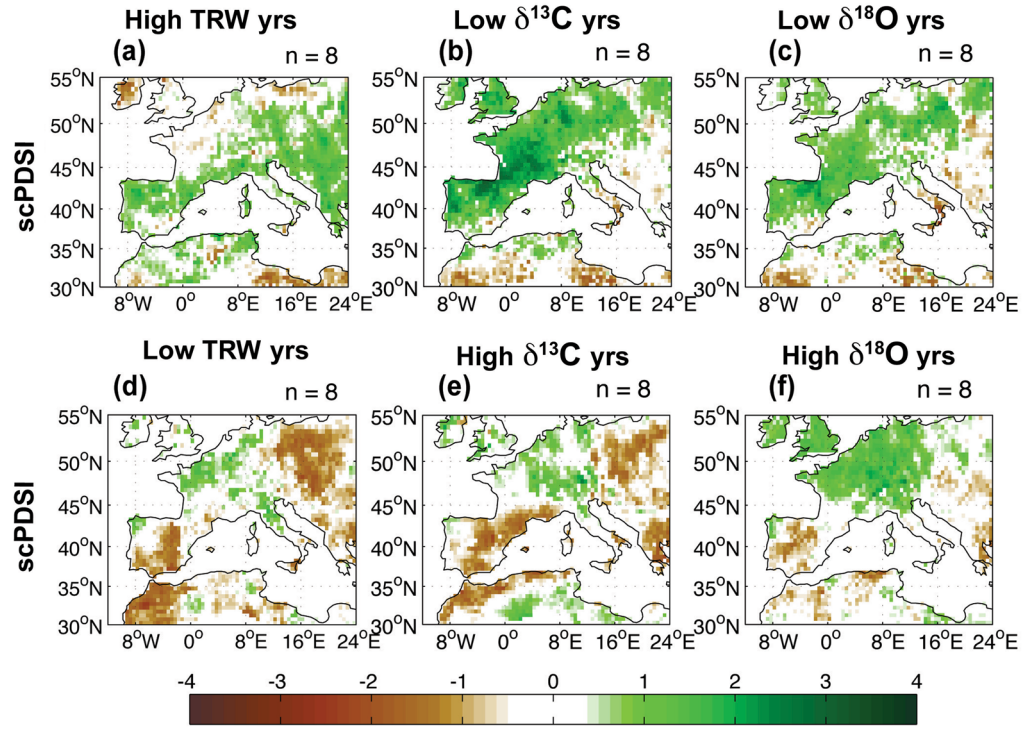

Fig. 11 As Fig. 8, but using the years detected by the 8 high/low proxy values from the instrumental period (1925–2002) for the self-calibrating Palmer Drought Severity Index (scPDSI) from the Old World Drought Atlas (OWDA)

8 Discussion

The persistent mid-nineteenth century pluvial seen in our reconstruction (Fig. 12) is corroborated by higher than usual precipitation levels reported between 1835 and 1875 in Barcelona (northeast IP) based on a recently published high-quality instrumental record (Prohom et al. 2015), with a 6-year record of rainy years (~1840s–1850s), unique in the next 160 years (Rodrigo and Barriendos 2008; Camuffo et al. 2013). Moreover, historical documentation also reported a lack of droughts and more frequent and severe catastrophic floods in the mid-nineteenth century in Iberia (Barriendos and Martin-Vide 1998; Llasat et al. 2005; Barriendos and Rodrigo 2006), ending this period of extreme floods with the 1874 Santa Tecla flash flood in Catalonia with more than 500 deaths (Ruiz-Bellet et al. 2015). This 19th century pluvial period is also confirmed by higher frequency of extreme events, such as strong snowstorms, marine storms, atmospheric convective activity and catastrophic floods, reported without a well-marked seasonality (Barriendos and Martin-Vide 1998). This unusual occurrence of wet years, associated with high atmospheric instability, may result from a prevalent meridional circulation associated with cold air aloft, which—upon contact with warm/humid air masses from the Mediterranean—may trigger torrential rainfall over the IP, especially over the northeastern IP (Barriendos and Martin-Vide 1998). These severe atmospheric events may also be associated with marked negative NAO phases and advection of cooler air aloft, producing strong rainfall events during such a 'cold phase' across the entire northern IP, and thus being detectable on both sides: northeastern (i.e. Mediterranean) and northwestern (i.e. Atlantic) IP, where our study site is located.

This information based on historic data aligns with the synoptic situation reported in our composite maps from the instrumental and pre-instrumental periods. During the instrumental period, low $\delta^{13}C$ and $\delta^{18}O$ years show circulation anomalies that are consistent with this interpretation with anomalous high SLP over Iceland and lower in the mid-latitudes (Fig. 6k, l), leading to anomalous northwesterly moisture transport from the Atlantic onto the IP (Fig. 6h, i). These circulation features are also associated with anomalous cool SAT across the broader IP (Fig. 6e, f). In the pre-instrumental period, the SLP anomaly pattern associated with low $\delta^{18}O$ years during this unusual pluvial period (Fig. 8c) is indicative of the negative NAO conditions suggested above.

Nevertheless, not all the atmospheric events occurred synchronically between the Atlantic and the Mediterranean sides of the northern IP. During the late Maunder Minimum (1675–1715) historic data based on Catholic rogation ceremonies from northeastern locations in Catalonia show almost no drought with steady precipitation levels (Barriendos 1997), whereas rogations from locations with a stronger Atlantic influence show drier conditions, such as Toledo and Zamora located in the western IP (Domínguez-Castro et al. 2010) and the Ebro basin (Vicente-Serrano and Cuadrat 2007). This situation may be linked to a prevalent anticyclone associated with cold conditions connected to dry weather in the Atlantic region, but with moderate precipitation levels in the Mediterranean side driven by moisture coming from the East. Consistently with the historical findings from the Atlantic side, our late spring–early

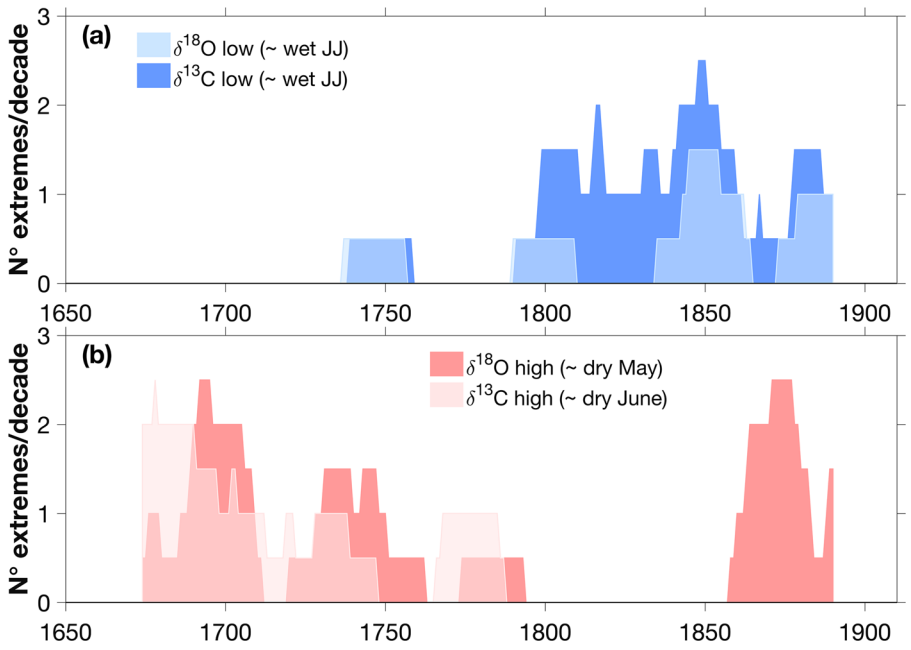

Fig. 12 Time-series of the number of extreme events in 20-year sliding windows for the extreme values in both $\delta^{13}C$ and $\delta^{18}O$ records. Wet (dry) conditions are reflected by low (high) isotopic extreme values

summer reconstruction (Fig. 12b) indicates higher occurrence of dry years detected by high values in both isotopic records during the late Maunder Minimum.

In contrast, other dry periods were co-occurring across the entire northern IP, as for example a drought during 1775–1778, evident in the Ebro basin under strong Atlantic influence (Vicente-Serrano and Cuadrat 2007). The anomalous climatic conditions extended along the Mediterranean coast and are considered among the strongest climatic irregularities occurring during the Maldà Oscillation in Catalonia, northeastern IP (Barriendos and Llasat 2003). This period was likely associated with sustained high pressure anomalies over central Europe (Luterbacher et al. 2000), which may have produced a 'blocking' situation preventing the arrival of low pressure systems from the Atlantic Ocean. In our high $\delta^{13}C$ years indicative of dry June conditions, the SLP anomalies (Figs. 7h, 8e) show comparable features to such a scenario, which could have led to prolonged droughts in the Western Mediterranean Basin, interspersed with flooding events (Barriendos and Llasat 2003).

Overall, our isotopic tree-ring reconstruction shows the most noticeable period with frequent dry summers from 1665 to 1700 considering the total extent spanning until 1900. In agreement, historical data from Toledo Cathedral based on rogations reported the most severe droughts occurring between 1576 and 1800, whereas almost no droughts were found during the 1800–1900 period (Dominguez-Castro et al. 2008). The fact that this period displays a lack of droughts agrees with the nineteenth century pluvial situation described in Fig. 12a. In addition, years with extreme values in the tree-ring proxies (Table 2) concur with some particular years of extreme droughts described by historical documentation, such as the years 1680 (Domínguez-Castro et al. 2010), 1753, 1817 or 1824 (Domínguez-Castro et al. 2012). Finally, the drought period detected by the isotopic tree-ring series during the second half of the nineteenth century is confirmed by historical proxies showing dry conditions for the Ebro basin during the same period, a strong positive NAO index at the end of the nineteenth and early twentieth century (Vicente-Serrano and Cuadrat 2007) and by instrumental records from Barcelona that show a dry spell from 1878 to 1919 (Prohom et al. 2015). From 1880 to 1910 extremely low grain production was reported in Spain that led to strong reductions in food availability during the first years of the twentieth century and related impacts as social conflict and migrations (Vicens Vives 1985; Blanco et al. 1986). Although starvation and migration are driven by a myriad of phenomena, including political and social factors, the dry period in the second half of the nineteenth century may have also played a role in this historically known crisis of subsistence and economic migrations due to hunger, such as the famous Galician and Asturian migration to South America (Ojeda and San Miguel 1985; Gómez Gómez 1996).

9 Conclusions

Independent sources (natural and historical) of past climate variability validate our findings that attribute the non-linear moisture signals recorded by extreme tree-ring values to distinct large-scale atmospheric patterns, and allow for targeted seasonal 400-year reconstructions of summer hydroclimate for extreme wet and dry conditions independently.

An almost symmetric seasonal moisture signal was recorded during years with highest/lowest $\delta^{13}C$ values, with precipitation anomalies being significant for similar months (Fig. 5e). This explains the robust and strong linear relationship between $\delta^{13}C$ and precipitation seen in correlations (Fig. 3b). An opposite behaviour may render the weaker precipitation signal held by the $\delta^{18}O$ series, which shows a much more marked seasonal asymmetry in its moisture signal (Fig. 5f). These analyses of extremes revealed that high/low proxy values do not necessarily correspond to mirror images in the atmospheric anomaly patterns, suggesting different drivers and seasonality associated with asymmetric moisture signatures in the proxies, and thus hampering the strength of their climate signal when linear approaches are used.

Severe flooding and droughts are likely to become more frequent with an intensifying water cycle in a warmer world (Wentz et al. 2007; Trenberth 2011; Hartmann et al. 2013). For sustainable water resources management, information about past hydroclimatic changes are needed. Our approach determining the frequency of extreme climatic conditions in the past is a step forward towards a more realistic range of past climate variability considering that the standard methodology based on linear regressions are biased towards the mean climate and often underestimate extremes (McCarroll et al. 2015). Extreme analyses point to a better mechanistic understanding of links between tree-ring proxies and large-scale atmospheric dynamics and can improve climate reconstructions based on proxies with asymmetric and non-stationary signals. Since this information is not available with a traditional linear approach, non-linear methods in palaeoclimate research are useful to overcome the complexity of reconstructing atmospheric features. The distinct seasonal signal in stable isotopes and ring-width supports multi-parameter approaches for advances in the field.

Acknowledgements We thank Oriol Bosch and Octavi Planells for their participation in sampling and laboratory work. Use of the following data sets is gratefully acknowledged: Global Precipitation

Climatology Centre data by the German Weather Service (DWD) accessed through http://gpcc.dwd.de; SAT by the Climate Research Unit at the University of East Anglia; NNR data provided by NOAA/OAR/ESRL PSD, Boulder, Colorado, USA, through their website http://www.cdc.noaa.gov; and the 20CR Project supported by the U.S. DOE, Office of Science Innovative and Novel Computational Impact on Theory and Experiment program, and Office of Biological and Environmental Research, and by the NOAA Climate Program Office. This research was partially supported by the EU project ISONET (Contract EV K2-2001-00237) and the EU FP6 project Millennium (GOCE 017008). L.A.H. was supported by the *Marie Curie International Outgoing Fellowship PIOF-GA-2009-253277* grant within the FP7-PEOPLE-2009-IOF program. CCU was supported by the *Penzance* and *John P. Chase Memorial Endowed Funds* and the *Investment in Science Fund* at WHOI. This is LDEO Contribution #8053.

References

Andreu-Hayles L (2007) Climate and atmospheric CO_2 effects on Iberian pine forests assessed by tree-ring chronologies and their potential for climatic reconstructions. University of Barcelona

Andreu L, Planells O, Gutiérrez E, Helle G, Schleser GH (2008) Climatic significance of tree-ring width and $\delta^{13}C$ in a Spanish pine forest network. Tellus Ser B Chem Phys Meteorol 60:771–781

Andreu-Hayles L, Planells O, Gutiérrez E, Muntan E, Helle G, Anchukaitis KJ, Schleser GH (2011) Long tree-ring chronologies reveal 20th century increases in water-use efficiency but no enhancement of tree growth at five Iberian pine forests. Glob Change Biol 17:2095–2112. doi:10.1111/j.1365-2486.2010.02373.x

Barbour MM (2007) Stable oxygen isotope composition of plant tissue: a review. Funct Plant Biol 34:83–94. doi:10.1071/FP06228

Barriendos M (1997) Climatic variations in the Iberian Peninsula during the late Maunder Minimum (AD 167–1715): an analysis of data from rogation ceremonies. Holocene 7:105–111. doi:10.1177/095968369700700110

Barriendos M, Llasat MC (2003) The case of the 'Maldá' anomaly in the western Mediterranean Basin (AD 1760–1800): an example of a strong climatic variability. Clim Change 61:191–216. doi:10.1023/a:1026327613698

Barriendos M, Martin-Vide J (1998) Secular climatic oscillations as indicated by catastrophic floods in the Spanish Mediterranean Coastal Area (14th 19th centuries). Clim Change 38:473–491. doi:10.1023/a:1005343828552

Barriendos M, Rodrigo FS (2006) Study of historical flood events on Spanish rivers using documentary data. Hydrol Sci J 51:765–783. doi:10.1623/hysj.51.5.765

Blanco A et al (1986) Historia de España Historia 16. ISBN 84-85229-81-9 edn, Madrid

Bladé I, Liebmann B, Fortuny D, Oldenborgh GJ (2011) Observed and simulated impacts of the summer NAO in Europe: implications for projected drying in the Mediterranean region. Clim Dyn 39:709–727. doi:10.1007/s00382-011-1195-x

Borella S, Leuenberger M, Saurer M (1999) Analysis of $\delta^{18}O$ in tree rings: wood-cellulose comparison and method dependent sensitivity. J Geophys Res Atmos 104:19267–19273

Buntgen U, Frank D, Grudd H, Esper J (2008) Long-term summer temperature variations in the Pyrenees. Clim Dyn 31:615–631. doi:10.1007/s00382-008-0390-x

Buwen D, Rowan TS, Tim W, Kevin H (2013) Variability of the North Atlantic summer storm track: mechanisms and impacts on European climate. Environ Res Lett 8:034037

Cai W, Cowan T, Thatcher M (2012) Rainfall reductions over Southern Hemisphere semi-arid regions: the role of subtropical dry zone expansion. Sci Rep. doi:10.1038/srep00702

Camuffo D et al (2013) Western Mediterranean precipitation over the last 300 years from instrumental observations. Clim Change 117:85–101. doi:10.1007/s10584-012-0539-9

Compo GP et al (2011) The twentieth century reanalysis project. Q J R Meteorol Soc 137:1–28. doi:10.1002/qj.776

Cook ER, Kairiukstis L (1990) Methods of dendrochronology in applications in the environmental sciences. Kluwer, Dordrecht

Cook ER, Peters K (1997) Calculating unbiased tree-ring indices for the study of climatic and environmental change. Holocene 7:359–368

Cook ER, D'Arrigo RD, Mann ME (2002) A well-verified, multiproxy reconstruction of the Winter North Atlantic Oscillation Index since a.d. 1400*. J Clim 15:1754–1764. doi:10.1175/1520-0442(2002)015<1754:awvmro>2.0.co;2

Cook ER et al (2015) Old World megadroughts and pluvials during the Common Era. Sci Adv. doi:10.1126/sciadv.1500561

De Luis M, Carlos Gonzalez-Hidalgo J, Longares LA, Stepanek P (2009) Seasonal precipitation trends in the Mediterranean Iberian Peninsula in second half of 20th century. Int J Climatol 29:1312–1323. doi:10.1002/joc.1778

Dominguez-Castro F, Santisteban JI, Barriendos M, Mediavilla R (2008) Reconstruction of drought episodes for central Spain from rogation ceremonies recorded at the Toledo Cathedral from 1506 to 1900. A methodological approach. Glob Planet Change 63:230–242. doi:10.1016/j.gloplacha.2008.06.002

Domínguez-Castro F, García-Herrera R, Ribera P, Barriendos M (2010) A shift in the spatial pattern of Iberian droughts during the 17th century. Clim Past 6:553–563. doi:10.5194/cp-6-553-2010

Domínguez-Castro F, Ribera P, García-Herrera R, Vaquero JM, Barriendos M, Cuadrat JM, Moreno JM (2012) Assessing extreme droughts in Spain during 1750–1850 from rogation ceremonies. Clim Past 8:705–722. doi:10.5194/cp-8-705-2012

Dorado Liñán I, Gutiérrez E, Andreu-Hayles L, Heinrich I, Helle G (2012) Potential to explain climate from tree rings in the south of the Iberian Peninsula. Clim Res 55:121–136. doi:10.3354/cr01126

Dorado Liñán I et al (2011) Pooled versus separate measurements of tree-ring stable isotopes. Sci Total Environ 409:2244–2251

Dorado Liñán I et al (2012) Estimating 750 years of temperature variations and uncertainties in the Pyrenees by tree-ring reconstructions and climate simulations. Clim Past 8:919–933. doi:10.5194/cp-8-919-2012

Dorado Liñán I et al (2015) Eight-hundred years of summer temperature variations in the southeast of the Iberian Peninsula reconstructed from tree rings. Clim Dyn 44:75–93. doi:10.1007/s00382-014-2348-5

Esper J et al (2015) Atlantic and Mediterranean synoptic drivers of central Spanish juniper growth. Theor Appl Climatol 121:571–579. doi:10.1007/s00704-014-1254-4

Farquhar GD, O'Leary MH, Berry JA (1982) On the relationship between carbon isotope discrimination and the intercellular carbon dioxide concentration in leaves. Aust J Plant Physiol 9:121–137

Fernández A, Génova M, Creus J, Gutiérrez E (1996) Dendroclimatological investigations covering the last 300 years in Central Spain. In: Dean JS, Meko DM, Swetman TW (eds) Tree rings, environment and humanity. RADIOCARBON, Tucson, pp 181–190

Frank DC et al (2015) Water-use efficiency and transpiration across European forests during the Anthropocene. Nat. Clim Change 5:579–583 doi:10.1038/nclimate2614. http://www.nature.com/nclimate/journal/v5/n6/abs/nclimate2614.html-supplementary-information

Friedman JH (1984) A variable span scatterplot smoother. Laboratory for Computational Statistics. Stanford University Technical report no. 5

Fritts H (1976) Tree rings and climate. Academic Press, New York
Gagen M, McCarroll D, Jalkanen R, Loader NJ, Robertson I, Young GHF (2012) A rapid method for the production of robust millennial length stable isotope tree ring series for climate reconstruction. Glob Planet Change 82 83:96–103. doi:10.1016/j.gloplacha.2011.11.006
García Antón M, Franco Múgica F, Maldonado J, Morla Juaristi C, Sainz Ollero H (1997) New data concerning the evolution of the vegetation in Lillo pinewood (Leon, Spain). J Biogeogr 24:929–934. doi:10.1046/j.1365-2699.1997.00181.x
Giorgi F (2006) Climate change hot-spots. Geophys Res Lett 33:L08707. doi:10.1029/2006GL025734
Giorgi F, Lionello P (2008) Climate change projections for the Mediterranean region. Glob Planet Change 63:90–104
Gómez Gómez P (1996) De Asturias a América, Cuba (1850–1930): la comunidad asturiana de, Cuba edn. Pedro Gómez Gómez, Oviedo
Hartmann DL et al (2013) Observations: atmosphere and surface. In: Stocker TF, Qin D, Plattner G-K, Tignor M, Allen SK, Boschung J, Nauels A, Xia Y, Bex V, Midgley PM (eds) Climate change 2013: the physical science basis. Contribution of working group I to the fifth assessment report of the intergovernmental panel on climate change. Cambridge University Press, Cambridge, UK and New York, NY, USA
Hernández A et al (2015) Sensitivity of two Iberian lakes to North Atlantic atmospheric circulation modes. Clim Dyn 45:3403–3417. doi:10.1007/s00382-015-2547-8
Hoerling M et al (2012) Anatomy of an extreme event. J Clim 26:2811–2832. doi:10.1175/jcli-d-12-00270.1
Hurrell JW (1995) Decadal trends in the North Atlantic oscillation: regional temperatures and precipitation. Science 269:676–679
Kalnay E et al (1996) The NCEP/NCAR 40-year reanalysis project. Bull Am Meteorol Soc 77:437–471. doi:10.1175/1520-0477(1996)077<0437:tnyrp>2.0.co;2
Karnauskas KB, Ummenhofer CC (2014) On the dynamics of the Hadley circulation and subtropical drying. Clim Dyn 42:2259–2269. doi:10.1007/s00382-014-2129-1
Kistler R et al (2001) The NCEP–NCAR 50-year reanalysis: monthly means CD-ROM and documentation. Bull Am Meteorol Soc 82:247–267. doi:10.1175/1520-0477(2001)082<0247:tnnyrm>2.3.co;2
Konter O, Holzkämper S, Helle G, Büntgen U, Saurer M, Esper J (2014) Climate sensitivity and parameter coherency in annually resolved $\delta^{13}C$ and $\delta^{18}O$ from *Pinus uncinata* tree-ring data in the Spanish Pyrenees. Chem Geol 377:12–19. doi:10.1016/j.chemgeo.2014.03.021
Labuhn I et al (2014) Tree age, site and climate controls on tree ring cellulose $\delta^{18}O$: a case study on oak trees from southwestern France. Dendrochronologia 32:78–89. doi:10.1016/j.dendro.2013.11.001
Lau WKM, Kim KM (2015) Robust Hadley circulation changes and increasing global dryness due to CO_2 warming from CMIP5 model projections. Proc Natl Acad Sci USA 112:3630–3635. doi:10.1073/pnas.1418682112
Laumer W, Andreu L, Helle G, Schleser GH, Wieloch T, Wissel H (2009) A novel approach for the homogenization of cellulose to use micro-amounts for stable isotope analyses. Rapid Commun Mass Spectrometry 23:1934–1940
Leavitt SW, Long A (1984) Sampling strategy for stable carbon isotope analyses of tree rings in pine. Nature 311:145–147
Lehmann J, Coumou D (2015) The influence of mid-latitude storm tracks on hot, cold, dry and wet extremes. Sci Rep 5:17491. doi:10.1038/srep17491
Linderholm HW, Folland CK, Walther A (2009) A multicentury perspective on the summer North Atlantic Oscillation (SNAO) and drought in the eastern Atlantic Region. J Quat Sci 24:415–425. doi:10.1002/jqs.1261
Llamas MR (2003) Lessons learnt from from the impact of the neglected role of groundwater in Spain's water policy. In: Sharhan AS, Wood WW (eds) Water resources perspectives: evaluation, management, and policy. Elsevier Science, Amsterdam, pp 63–81
Llasat M-C, Barriendos M, Barrera A, Rigo T (2005) Floods in Catalonia (NE Spain) since the 14th century. Climatological and meteorological aspects from historical documentary sources and old instrumental records. J Hydrol 313:32–47. doi:10.1016/j.jhydrol.2005.02.004
Loader NJ, Robertson I, Barker AC, Switsur VR, Waterhouse JS (1997) ogy. Chem Geol 136:313–317
Loader NJ, Young GHF, Grudd H, McCarroll D (2013) Stable carbon-isotopes from Torneträsk, northern Sweden provide a millenni-allength reconstruction of summer sunshine and its relationship toArctic circulation. Quatern Sci Rev 62:97–113. doi:10.1016/j.quascirev.2012.11.014
López-Moreno JI, Beguería S, Vicente-Serrano SM, García-Ruiz JM (2007) Influence of the North Atlantic Oscillation on water resources in central Iberia: precipitation, streamflow anomalies, and reservoir management strategies. Water Resour Res 43:W09411. doi:10.1029/2007wr005864
Lu J, Vecchi GA, Reichler T (2007) Expansion of the Hadley cell under global warming. Geophys Res Lett 34:L06805. doi:10.1029/2006gl028443
Lu J, Deser C, Reichler T (2009) Cause of the widening of the tropical belt since 1958. Geophys Res Lett. doi:10.1029/2008gl036076
Luterbacher J et al (2000) Monthly mean pressure reconstruction for the Late Maunder Minimum Period (AD 1675–1715). Int J Climatol 20:1049–1066
Luterbacher J et al (2002) Reconstruction of sea level pressure fields over the Eastern North Atlantic and Europe back to 1500. Clim Dyn 18:545–561. doi:10.1007/s00382-001-0196-6
Manrique E, Fernandez-Cancio A (2000) Extreme climatic events in dendroclimatic reconstructions from spain. Clim Change 44:123–138
McCarroll D, Loader NJ (2004) Stable isotopes in tree rings. Quatern Res Rev 23:771–801
McCarroll D, Pawellek F (1998) Stable carbon isotope ratios of latewood cellulose in *Pinus sylvestris* from northern Finland: variability and signal-strength. Holocene 8:675–684. doi:10.1191/095968398675987498
McCarroll D et al (2009) Correction of tree ring stable carbon isotope chronologies for changes in the carbon dioxide content of the atmosphere. Geochim Cosmochim Acta 73:1539–1547. doi:10.1016/j.gca.2008.11.041
McCarroll D, Young GH, Loader NJ (2015) Measuring the skill of variance-scaled climate reconstructions and a test for the capture of extremes. Holocene 25:618–626. doi:10.1177/0959683614565956
Meko DM, Touchan R, Anchukaitis KJ (2011) Seascorr: a MATLAB program for identifying the seasonal climate signal in an annual tree-ring time series. Comput Geosci 37:1234–1241. doi:10.1016/j.cageo.2011.01.013
Melvin TM, Briffa KR (2008) A ""signal-free"" approach to dendroclimatic standardisation. Dendrochronologia 26:71–86
Mitchell TD, Jones PD (2005) An improved method of constructing a database of monthly climate observations and associated high-resolution grids. Int J Climatol 25:693–712
Naulier M et al (2015) A millennial summer temperature reconstruction for northeastern Canada using oxygen isotopes in subfossil trees. Clim Past 11:1153–1164. doi:10.5194/cp-11-1153-2015
Nicault A, Alleaume S, Brewer S, Carrer M, Nola P, Gutierrez E, Edouard JL, Urbinati C, Guiot J (2008) Mediterranean drought fluctuation during the last 500 years based on tree-ring data. Clim Dyn 31:227–245. doi:10.1007/s00382-007-0349-3

Ojeda G, San Miguel JL (1985) Campesinos, emigrantes, indianos Emigración y economía en Asturias, 1830–1930. Salinas, Ed. Ayalga. ISBN: 84-7411-132-3

Orden Martín R (2013) El pinar de Lillo. Bedia Artes Gráficas, S. C. Santander (Cantabria, Spain). ISBN: 978-84-695-6855-2

Pauling A, Luterbacher J, Casty C, Wanner H (2006) Five hundred years of gridded high-resolution precipitation reconstructions over Europe and the connection to large-scale circulation. Clim Dyn 26:387–405

Planells O, Gutiérrez E, Helle G, Schleser G (2009) A forced response to twentieth century climate conditions of two Spanish forests inferred from widths and stable isotopes of tree rings. Clim Change 97:229–252. doi:10.1007/s10584-009-9602-6

Previdi M, Liepert BG (2007) Annular modes and Hadley cell expansion under global warming. Geophys Res Lett 34:L22701. doi:10.1029/2007gl031243

Prohom M, Barriendos M, Sanchez-Lorenzo A (2015) Reconstruction and homogenization of the longest instrumental precipitation series in the Iberian Peninsula (Barcelona, 1786–2014). Int J Climatol. doi:10.1002/joc.4537

Rodó Baert E, Comin FA (1997) Variations in seasonal rainfall in Southern Europe during the present century: relationship with the North Atlantic Oscillation and the El Niño-Southern Oscillation. Clim Dyn 13:275–284

Rodrigo FS, Barriendos M (2008) Reconstruction of seasonal and annual rainfall variability in the Iberian peninsula (16th–20th centuries) from documentary data. Global Planet Change 63:243–257. doi:10.1016/j.gloplacha.2007.09.004

Rodriguez-Puebla C, Encinas AH, Nieto S, Garmendia J (1998) Spatial and temporal patterns of annual precipitation variability over the Iberian Peninsula. Int J Climatol 18:299–316

Ruiz-Bellet JL, Balasch JC, Tuset J, Barriendos M, Mazon J, Pino D (2015) Historical, hydraulic, hydrological and meteorological reconstruction of 1874 Santa Tecla flash floods in Catalonia (NE Iberian Peninsula). J Hydrol 524:279–295. doi:10.1016/j.jhydrol.2015.02.023

Saurer M, Schweingruber F, Vaganov EA, Shiyatov SG, Siegwolf R (2002) Spatial and temporal oxygen isotope trends at the northern tree-line in Eurasia. Geophys Res Lett 29:7-1–7-4. doi:10.1029/2001GL013739

Saurer M et al (2014) Spatial variability and temporal trends in water-use efficiency of European forests. Glob Change Biol 20:3700–3712. doi:10.1111/gcb.12717

Schneider U, Becker A, Finger P, Meyer-Christoffer A, Ziese M, Rudolf B (2014) GPCC's new land surface precipitation climatology based on quality-controlled in situ data and its role in quantifying the global water cycle. Theoret Appl Climatol 115:15–40. doi:10.1007/s00704-013-0860-x

Seftigen K, Linderholm HW, Loader NJ, Liu Y, Young GHF (2011) The influence of climate on $^{13}C/^{12}C$ and $^{18}O/^{16}O$ ratios in tree ring cellulose of *Pinus sylvestris* L. growing in the central Scandinavian Mountains. Chem Geol 286:84–93. doi:10.1016/j.chemgeo.2011.04.006

Tejedor E, de Luis M, Cuadrat J, Esper J, Saz M (2015) Tree-ring-based drought reconstruction in the Iberian Range (east of Spain) since 1694. Int J Biometeorol. doi:10.1007/s00484-015-1033-7

Trenberth K (2011) Changes in precipitation with climate change. Clim Res 47:123–138. doi:10.3354/cr00953

Treydte K et al (2007) Signal strength and climate calibration of a European tree-ring isotope network. Geophys Res Lett 34:L24302. doi:10.1029/2007gl031106

Trigo RM, Pozo-Vázquez D, Osborn TJ, Castro-Díez Y, Gámiz-Fortis S, Esteban-Parra MJ (2004) North Atlantic oscillation influence on precipitation, river flow and water resources in the Iberian Peninsula. Int J Climatol 24:925–944. doi:10.1002/joc.1048

Trigo RM, Valente MA, Trigo IF, Miranda PMA, Ramos AM, Paredes D, García-Herrera R (2008) The impact of North Atlantic wind and cyclone trends on European precipitation and significant wave height in the Atlantic. Ann N Y Acad Sci 1146:212–234. doi:10.1196/annals.1446.014

Vicens Vives J (1985) Historia económica de España. In: ISBN: 84-316-1106-5 edn. Vicens Vives Ed., Barcelona, 8th edn, p 782

Vicente-Serrano SM (2006) Spatial and temporal analysis of droughts in the Iberian Peninsula (1910–2000). Hydrol Sci J 51:83–97. doi:10.1623/hysj.51.1.83

Vicente-Serrano SM, Cuadrat JM (2007) North Atlantic oscillation control of droughts in north-east Spain: evaluation since 1600 AD. Clim Change 85:357–379. doi:10.1007/s10584-007-9285-9

Vicente-Serrano SM, López-Moreno JI (2008) Nonstationary influence of the North Atlantic Oscillation on European precipitation. J Geophys Res Atmos 113:D20120. doi:10.1029/2008jd010382

Wentz FJ, Ricciardulli L, Hilburn K, Mears C (2007) How much more rain will global warming bring? Science 317:233–235. doi:10.1126/science.1140746

Wigley TML, Briffa KR, Jones PD (1984) On the average value of correlated time series, with applications in dendroclimatoly and hydrometeorology. J Clim Appl Meteorol 23:201–213

Young GHF et al (2015) Oxygen stable isotope ratios from British oak tree-rings provide a strong and consistent record of past changes in summer rainfall. Clim Dyn 45:3609–3622. doi:10.1007/s00382-015-2559-4